PHILOSOPHICAL TRANSACTIONS OF THE ROYAL SOCIETY A

rsta.royalsocietypublishing.org

Research

Cite this article: Koskinen TT, Lavvas P, Harris MJ, Yelle RV. 2014 Thermal escape from extrasolar giant planets. *Phil. Trans. R. Soc. A* **372**: 20130089.
http://dx.doi.org/10.1098/rsta.2013.0089

One contribution of 17 to a Theo Murphy Meeting Issue 'Characterizing exoplanets: detection, formation, interiors, atmospheres and habitability'.

Subject Areas:
extrasolar planets

Keywords:
extrasolar planets, hydrodynamics, atmospheric physics

Author for correspondence:
Tommi T. Koskinen
e-mail: tommi@lpl.arizona.edu

Royal Society Publishing

Thermal escape from extrasolar giant planets

Tommi T. Koskinen[1], Panayotis Lavvas[2], Matthew J. Harris[3] and Roger V. Yelle[1]

[1]Lunar and Planetary Laboratory, University of Arizona, 1629 E. University Boulevard, Tucson, AZ 85721-0092, USA
[2]Groupe de Spectrométrie Moléculaire et Atmosphérique, UMR CNRS 6089, Université Reims Champagne-Ardenne, 51687 Reims, France
[3]Department of Physics and Astronomy, University College London, Gower Street, London WC1E 6BT, UK

The detection of hot atomic hydrogen and heavy atoms and ions at high altitudes around close-in extrasolar giant planets (EGPs) such as HD209458b implies that these planets have hot and rapidly escaping atmospheres that extend to several planetary radii. These characteristics, however, cannot be generalized to all close-in EGPs. The thermal escape mechanism and mass loss rate from EGPs depend on a complex interplay between photochemistry and radiative transfer driven by the stellar UV radiation. In this study, we explore how these processes change under different levels of irradiation on giant planets with different characteristics. We confirm that there are two distinct regimes of thermal escape from EGPs, and that the transition between these regimes is relatively sharp. Our results have implications for thermal mass loss rates from different EGPs that we discuss in the context of currently known planets and the detectability of their upper atmospheres.

1. Introduction

The upper atmospheres of three different extrasolar giant planets (EGPs)—HD209458b, HD189733b and WASP-12b—were recently probed by UV transit observations obtained by the Hubble Space Telescope (HST) [1–6]. These observations indicate that close-in EGPs such as HD209458b are surrounded by a hot thermosphere composed of atomic hydrogen that extends to several planetary radii and provide the required line of

sight optical depth in the atomic resonance lines to explain large transit depths [7–9]. It is also widely believed that the atmospheres of close-in EGPs undergo hydrodynamic escape [10,11].

The term hydrodynamic escape is commonly associated with transonic outflow [12]. However, recent calculations by Koskinen *et al.* [8] demonstrate that the altitude of the sonic point is strongly dependent on radiative transfer and heating rates in the upper atmosphere. Furthermore, they show that on planets such as HD209458b the temperature gradient in the upper atmosphere is close to adiabatic and thus the sonic point is likely to be located at a relatively high altitude. On the other hand, the altitude of the sonic point may also depend on poorly known factors such as tidal forces, interaction with the stellar wind and the strength of the possible planetary magnetic field [13–15]. This means that the location of the sonic point in models of thermal escape is mostly of theoretical interest. The currently available observations do not have adequate signal to noise (S/N) or wavelength resolution to allow for the location of the sonic point to be determined on actual planets. What is clear, however, is that rapid escape on close-in EGPs affects the temperature and density profiles in their atmospheres, and that escape from their atmospheres can be roughly modelled with fluid equations. In line with Tian *et al.* [16,17], we consider this as the hydrodynamic escape regime.

Needless to say, the thermospheres of the giant planets in the Solar System differ significantly from this picture. For instance, the exobase on Jupiter is located only approximately 2300 km above the 1 bar level [18], whereas on Saturn it is located only 2700–3000 km above the 1 bar level [19]. In both cases, the thermal escape parameter $X = GM_{\mathrm{p}}m/kTr_{\mathrm{exo}}$ is large, between 250 and 450, and thermal escape is firmly in the classical Jeans regime based on kinetic theory [20,21]. In this case, escape does not affect the temperature and density structure of the atmosphere significantly, and proceeds on a particle-by-particle basis from the exobase into the nearly collisionless exosphere. Given this background, it is interesting to assess how the escape mechanism and thermal escape rates on different EGPs orbiting Sun-like stars vary with orbital distances. The upper atmospheres of close-in giant planets are heated by the stellar UV radiation, and at some orbital distance the flux should be high enough to cause a transition from kinetic escape to hydrodynamic escape.

Koskinen *et al.* [22,23] used results from a three-dimensional model for the thermospheres of EGPs to argue that this transition, which is controlled by the dissociation of H_2 below the exobase, and the subsequent lack of efficient infrared cooling by H_3^+ occurs within a surprisingly narrow range of orbital distances between 0.1 and 0.2 AU for Jupiter-type planets orbiting Sun-like stars. In other words, there is a relatively sharp limit to the incoming UV flux that causes the atmosphere to expand and begin to undergo rapid escape. These calculations also indicate that the upper atmospheres of close-in EGPs are quite resilient—they remain relatively cool and stable at surprisingly small orbital distances. The results provide an important perspective on the predicted properties of the several hundreds of known EGPs, and can be used to guide statistical studies of mass loss from EGPs [24,25] as well as to search for good targets for future observations of their upper atmospheres.

Previous work by Koskinen *et al.* [22,23] relied on a model composed exclusively of hydrogen and helium. However, recent calculations have shown that the photochemistry of carbon and oxygen species may play an important role in controlling the composition in the upper atmosphere of HD209458b [26]. In particular, complex photochemistry in a solar composition atmosphere can lead to significant dissociation of H_2 by OH radicals at a relatively deep pressure level of 1 μbar. It should be noted that on both Jupiter and Saturn the thermosphere is composed mostly of H_2 up to the exobase that is located at a pressure of a few pbar, so this is another important difference between close-in EGPs and the giant planets in the Solar System.

In this paper, we update the previous calculations of Koskinen *et al.* [22,23] to include more complex photochemistry. More specifically, we study the dissociation chemistry of H_2 as a function of orbital distance on EGPs by relying on existing thermal structure calculations and new photochemical calculations. We use the results to assess the escape mechanism and mass loss rates under different levels of irradiation based on new theoretical results

[20,21] and their application to close-in EGPs [8,9]. We then proceed to generalize the results to a sample of known EGPs to make specific predictions about the nature of their upper atmospheres.

2. Methods

We studied the dissociation chemistry of H_2 by using the photochemical model of Lavvas *et al*. [27,28] that was recently modified to simulate the atmospheres of gas giant planets at high temperatures [8,9]. In addition to the reaction rate coefficients, the required inputs for the photochemical model are the stellar spectrum, a temperature–pressure (T–P) profile and the eddy diffusion coefficient K_{zz} that generally depends on altitude. In the lower atmosphere, we used T–P profiles from Sudarsky *et al*. [29] and Burrows *et al*. [30] that were calculated for EGPs at orbital distances ranging from 0.1 to 1 AU. We calculated the composition at 1, 0.5, 0.4, 0.3, 0.2, 0.1 and 0.047 AU. For HD209458b, we used the T–P profile from Showman *et al*. [31]. The T–P profiles above the 1 µbar level of each simulation were adopted from Koskinen *et al.* [22,23] for different orbital distances, and connected smoothly with the T–P profiles at lower altitudes. We estimated the terminal values of K_{zz} in the upper atmosphere based on the simple scaling proposed by Koskinen *et al.* [32]. These values range from 10^3 to $10^4\,m^2\,s^{-1}$ between 1 and 0.047 AU, respectively. The reader should note that these values are more conservative than the relatively high values typically presented in the literature [26].

We then proceeded to use the results from the photochemical model as lower boundary conditions for the escape model at the 1 µbar level, and recalculated the temperature, density and velocity profiles in the thermosphere. For this purpose, we used the one-dimensional escape model of Koskinen *et al.* [8,9]. We fixed the lower boundary temperature of this model to a value consistent with the T–P profiles above. The lower boundary was placed at 1 µbar, because most of the extreme-ultraviolet (EUV) radiation that powers escape in the model is absorbed above this level. The reader should note that X-rays typically penetrate deeper than the 1 µbar level and accounting for their heating impact on the atmosphere requires a model of radiative transfer that includes cooling by the abundant molecules. At the upper boundary, we applied either the modified Jeans or Jeans conditions, depending on the value of X. In both cases, we included the ambipolar electric potential that can be important in ionized atmospheres [8,33]. Our model is self-consistent with regard to these boundary conditions in that the altitude of the exobase is updated regularly during the simulation, and the Jeans conditions are applied slightly below the exobase where the Knudsen number $Kn \approx 0.1$. In this way, the model develops to a steady state with a converged altitude for the exobase, when an exobase exists at a reasonably low altitude. At close-in orbits, the exobase extends to very high altitudes, and the modified Jeans conditions are compatible with the outflow boundary conditions [8].

3. Results

(a) Hydrogen dissociation chemistry

The photochemical calculations constrain the mixing ratio of H at the 1 µbar lower boundary of the hydrodynamic escape model. The latter also includes the ion chemistry of H_2, H and He with a reaction scheme similar to that of Yelle [11] and Koskinen *et al.* [34]. With an accurate lower boundary constraint, the escape model can therefore update the H_2/H transition level based on the temperature and chemistry in the thermosphere, as long as the homopause is located reasonably near the 1 µbar level. Our calculations show that the mixing ratio of H at the 1 µbar level varies from about 4.9×10^{-3} at 1 AU to about 1.7×10^{-1} at 0.1 AU, finally reaching about 0.5 for HD209458b. As a point of comparison, the corresponding mixing ratio at Jupiter is about 10^{-3} [35]. Interestingly, H_2 is mostly dissociated thermally at orbital distances greater than 0.1 AU.

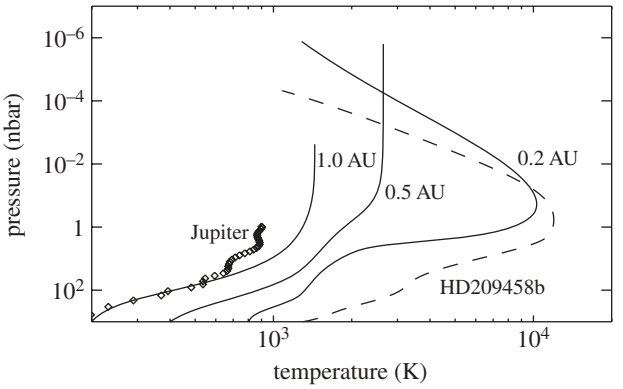

Figure 1. Simulated temperature–pressure profiles for EGPs with planetary parameters of HD209458b at different orbital distances (solid lines). The T–P profiles are shown up to the exobase when it exists (at orbital distances greater than 0.3 AU). Also shown are the T–P profiles for Jupiter [35] and the simulated profile for HD209458b [8,9].

At close-in orbits, within 0.1 AU, H_2 can also be dissociated by OH radicals that are released by the photolysis of water molecules [26]. Because this dissociation mechanism is primarily driven by far-ultraviolet (FUV) radiation, which penetrates past the EUV heating peak, it can potentially dissociate H_2 at a deeper pressure level than thermal dissociation. We note, however, that the relative importance of thermal dissociation and photochemistry depends on the assumed T–P profile. The dayside T–P profile typically assumed for HD209458b, which was also used in this work, is warm enough to dissociate thermospheric H_2 anyway.

At 1 AU, the H_2/H transition occurs above the 0.2 nbar level, i.e. above the thermospheric heating peak that is located at 1–10 nbar. Near the exobase at 2.4 pbar, the mixing ratio of H is close to unity. This means that there is a rather sharp H_2/H transition at low pressures near the exobase, but that H_2 is the dominant species in most of the thermosphere. Moving inwards from 1 to 0.4 AU, the H_2/H dissociation front moves down to the 3 nbar level. By 0.3 AU, it reaches down to the 20 nbar level, i.e. below the EUV heating peak. At this point, the thermosphere also heats up and expands dramatically (see §3*b*). At 0.2 AU, the exobase is above the 16 R_p upper boundary and the maximum temperature is 10 300 K. At 0.1 AU, the H_2/H transition is located near the 50 nbar level and, as we pointed out above, for HD209458b, this transition takes place near the 1 μbar level.

(b) Temperature and velocity

Figure 1 shows the T–P profiles from our new calculations for different orbital distances above the 1 μbar level. These calculations are based on the planetary parameters of HD209458b. The results are compared with the model T–P profile for HD209458b [8,9] and the measured equatorial T–P profile for Jupiter [35]. At 1 AU, the exospheric temperature is $T_\infty \approx 1440$ K. In general, the temperature increases rather steeply with altitude between 0.1 and 100 nbar in a region where most of the stellar EUV radiation is absorbed. At 1 AU, stellar heating and conduction dominate the energy balance. In particular, at high altitudes, heating is almost exactly balanced by conduction, leading to an isothermal temperature profile. Similar to Jupiter, radiative cooling by H_3^+ is also important near the heating and ionization peak. Contrary to HD209458b, cooling by adiabatic expansion or advection is negligible.

The exospheric temperature at 1 AU is comparable to the exospheric temperature on Earth. The model T–P profile at 1 AU is also similar to the observed T–P profile on Jupiter. In particular, our temperature profile agrees well with the Jovian profile below the 20 nbar level. It is well known that the temperatures on Jupiter and other giant planets in the Solar System are higher than expected from solar heating alone [36], and the heating mechanism responsible for this

is currently unknown. In this regard, it is interesting that the correct T–P profile in the lower thermosphere can be obtained by moving Jupiter from 5 to about 1 AU, i.e. by multiplying the solar flux by a factor of 25.

It is not easy to predict the degree to which the atmospheres of EGPs might also be warmer than expected from solar heating. The situation in the Solar System may provide some guidance on this though. The leading suggestions for the missing heating mechanism on Jupiter and Saturn include redistribution of auroral energy from the poles to the Equator or, given the rapid rotation of these planets and polar ion drag that may constrain the auroral energy to high latitudes, direct heating by breaking gravity waves [37,38]. Both of these phenomena are observed on Earth, but solar EUV heating is still the most important overall energy source in the thermosphere, and the temperature in the Earth's thermosphere can easily be explained. It may thus be argued that stellar heating simply overtakes any secondary heat sources within 1 AU. We rely on this assumption in this work, and present results within 1 AU based on stellar heating only.

Adiabatic cooling or advection that are associated with the escape of the atmosphere do not affect the energy balance at 1 AU. The 'critical' thermal escape parameter at the exobase ($r_\infty = 1.09$ R_p) is $X_\infty = 72$, and near the EUV heating peak $X = 190$. These values imply a negligible mass loss rate of $\dot{M} \approx 3.7 \times 10^{-23}\,\mathrm{kg\,s^{-1}}$. We note that the thermospheric heating efficiency at 1 AU, which is based on the balance of radiative (photoelectron) heating and cooling, is about $\eta_{\mathrm{eff}} = 0.48$. This value is not very different from $\eta_{\mathrm{eff}} = 0.44$ that we estimated for HD209458b.[1] Thus, the energy-limited mass loss rate at 1 AU is about $10^4\,\mathrm{kg\,s^{-1}}$. This means that the escape rate that we calculated at 1 AU is technically not in the energy-limited regime—instead, it is many orders of magnitude lower than the energy-limited rate. We argue in §3*c* that this apparent discrepancy arises from a confusion about the definition of heating efficiency rather than any new insights into the physics of evaporation.

Moving inwards from 1 to 0.5 AU, the exospheric temperature increases from 1440 to about 2630 K. With this increase in temperature, the exobase extends to about 1.8 R_p, where the pressure is about 7×10^{-7} nbar. Such a low pressure for the exobase is possible because the thermosphere is mostly ionized at radii higher than about 1.4 R_p, and the cross section for Coulomb or ion-neutral collisions is much larger than the cross section for neutral–neutral collisions. This is in contrast to 1 AU where the electron–neutral mixing ratio at the exobase is only $x_e = 6 \times 10^{-3}$. As shown in figure 1, the temperature profile at 0.5 AU is isothermal near the exobase, indicating that heating is balanced by conduction. Similar to 1 AU, escape has a negligible impact on the T–P profile, and the modified Jeans outflow velocity at the exobase is only $v_{J\infty} = 1.9 \times 10^{-6}\,\mathrm{m\,s^{-1}}$. The critical escape parameter, in this case, is $X_\infty = 26$. In addition to conduction, cooling from H_3^+ plays a substantial role in the lower thermosphere. This can be seen in the shape of the T–P profile (figure 1) near the 10 nbar level and below where infrared cooling is comparable to the stellar heating rate.

At 0.4 AU, the exospheric temperature is 2840 K, i.e. only slightly higher than at 0.5 AU, and the critical escape parameter is $X_\infty = 20$. Inwards from 0.4 AU, the atmosphere undergoes an interesting transition. For instance, at 0.2 AU (figure 1), the maximum temperature is much higher than at 0.4 AU, reaching about 10 300 K at 1.4 R_p, and formally the exobase is located above the 16 R_p upper boundary of the model. Above 1.4 R_p, the temperature also decreases with altitude. This is because heating at high altitudes is no longer balanced by conduction—instead, it is balanced by 'adiabatic' cooling that is associated with the expansion and escape of the atmosphere. In this sense, the model at 0.2 AU is qualitatively similar to HD209458b where the same behaviour has been predicted by several previous models [8,9,11,33]. Based on these changes in the location of the exobase and the energy balance, we argue that the transition to 'hydrodynamic' escape occurs near 0.3 AU. We note that a similar transition was also identified by Tian *et al*. [16,17] in the context of the early terrestrial atmosphere.

[1]Note that these efficiencies are defined in terms of the stellar flux at wavelengths shorter than 912 Å.

(c) Escape rates and mixing

The energy-limited loss rate in the context of extrasolar planets is often formulated as [13,25]

$$\dot{L} = \frac{\eta \pi r_{\mathrm{EUV}}^2 F_{\mathrm{EUV}}}{\Phi_0}, \tag{3.1}$$

where r_{EUV} is the radius of the EUV heating peak, F_{EUV} is the stellar EUV flux, Φ_0 is the gravitational potential and η is referred to as the 'heating efficiency'. We believe that the use of 'heating efficiency' here can be misleading.[2] For instance, the peak midday heating efficiency of the Earth's thermosphere is 50–55% [39] but only a tiny fraction of the energy that heats the thermosphere powers escape. Instead, the heating is mostly balanced by downwards heat conduction, radiative cooling and to some degree by circulation. Under these circumstances, a reasonable estimate of the temperature profile can be derived analytically from a simple balance between stellar heating and conduction [10,40]. Naturally, these considerations are different on Earth, in any case, because the escape of lighter species such as H and H_2 is diffusion limited, but the discussion here illustrates the general limitations of the energy limit.

With a proper choice of η, r_{EUV} and Φ_0, equation (3.1) is always accurate and with $\eta = 1$ it yields an upper limit on thermal escape rates. It is thus better to call η 'mass loss efficiency' rather than 'heating efficiency'. This better reflects the fact that equation (3.1) describes a balance between external heating and cooling by adiabatic expansion [11]. It also removes any apparent disagreement between equation (3.1) and our results at 0.4–1 AU in §3*b*. If one accounts for the fact that heating is mostly balanced by downwards conduction, the mass loss efficiency is much lower than the heating efficiency. Despite the consistency introduced by the new definition of η, equation (3.1) is actually not very useful unless adiabatic cooling really is important. It may always be possible to tune the mass loss efficiency to force the equation to agree with modelled or observed mass loss rates, but this does not capture the relevant physics in all cases. Thus, the escape mechanism must also be studied in detail before energy-limited escape can be assumed.

The globally averaged mass loss rates are 3.4×10^{-6} and $6.3 \times 10^{-5}\,\mathrm{kg\,s^{-1}}$ at 0.5 and 0.4 AU, respectively. Needless to say, these mass loss rates are irrelevant to the long-term evolution of the atmosphere. At 0.2 AU, the mass loss rate is $8 \times 10^5\,\mathrm{kg\,s^{-1}}$. In this case, the heating efficiency is comparable, although not identical, to the mass loss efficiency. According to our simulations, the heating efficiency is about 8.5% at 0.2 AU. This relatively low value arises because cooling from H_3^+ is important in the lower thermosphere below the H_2/H transition. The T–P profile at 0.1 AU is qualitatively similar to the T–P profile at 0.2 AU, and the maximum temperature is about 10 900 K. The mass loss rate at 0.1 AU is about $6 \times 10^6\,\mathrm{kg\,s^{-1}}$. The heating efficiency at 0.1 AU is only 22% because H_3^+ still cools the lower thermosphere. As we argue below, this cooling effect becomes negligible within 0.1 AU, and thus the heating efficiency for HD209458b increases to 44%. As before, we obtained a mass loss rate of $4.1 \times 10^7\,\mathrm{kg\,s^{-1}}$ from our reference model of HD209458b [8,9].

Our results show that heavy species such as C, O and Si that collide frequently with H and H^+ escape the atmosphere of HD209458b with nearly uniform mixing ratios in the thermosphere [8,9]. There is an obvious interest in estimating the degree to which this is true on other EGPs, because escape can affect the composition and thus the evolution of the atmosphere. For example, the thermal mass loss rate predicted by us and previous models of HD209458b [11] implies that the planet has lost less than 1% of its mass during the lifetime of the stellar system. However, it also implies that HD209458b loses the equivalent mass of its whole atmosphere above the 1 bar level approximately every 800 000 years.

The cross-over mass equation given by Hunten *et al.* [41] can be used to derive a rough estimate of the limiting mass loss rate $\dot{M}_{\mathrm{lim}}$ that is required for a species with mass M_{c} (in units of m_{H}) to

[2]Note that heating efficiency is often understood as the fraction of solar energy that heats the atmosphere.

escape with H owing to neutral–neutral collisions

$$\dot{M}_{\rm lim} = 4\pi m_{\rm H}^2 G M_{\rm p} (M_{\rm c} - 1) \frac{nD_{\rm c}}{kT}, \tag{3.2}$$

where $D_{\rm c}$ is the mutual diffusion coefficient for species c with H. At a temperature of 7200 K [8,9], the mass loss rate required to mix He is about $10^6\,{\rm kg\,s^{-1}}$, whereas the mass loss rate required to mix C and O is 4–6 $\times\, 10^6\,{\rm kg\,s^{-1}}$. Given that we estimate a mass loss rate of $6 \times 10^6\,{\rm kg\,s^{-1}}$ at 0.1 AU, progressively heavier neutral species escape the atmosphere with decreasing orbital distance from 0.1 AU. Because carbon species are effective in removing H_3^+, this is another indication that infrared cooling is not effective in the lower thermospheres of close-in EGPs. Instead, H_2 is dissociated near the 1 μbar level, and the temperature increases rapidly with altitude above this level.

(d) The effect of gravitational potential

The escape mechanism depends on the gravitational potential Φ through its dependence on X. The energy-limited escape rate given by equation (3.1) and the cross-over mass loss rate given by equation (3.2) also depend on the gravitational potential. For example, Koskinen *et al.* [34] pointed out that the atmospheres of heavy planets such as HD17156b are not likely to undergo rapid escape even at close-in orbits. We explored the effect of Φ in more detail by generating models at the same orbital distances as before but with different values of the surface potential ranging from 0.1 to 3 $\Phi_{\rm J}$, where $\Phi_{\rm J}$ is the surface potential of Jupiter. In order to illustrate the results, we discuss them in the context of a few well-known transiting EGPs. For instance, GJ3470b is a nearby Neptune-sized planet orbiting an M dwarf that has a gravitational potential of about 0.1 $\Phi_{\rm J}$. The gravitational potential of HD209458b is 0.5 $\Phi_{\rm J}$, i.e. similar to that of Saturn, whereas the gravitational potential of HD189733b is identical to that of Jupiter. The gravitational potential of HD17156b, on the other hand, is 2.9 $\Phi_{\rm J}$. More details on these planets are available, for instance, at www.exoplanet.eu.

The model for HD189733b at 0.2 AU is qualitatively similar to the corresponding model for HD209458b, with a peak temperature of 10 100 K. However, at 0.3 AU, the model for HD189733b is similar to the model of HD209458b at 0.5 AU, with an isothermal temperature of only 2700 K near the exobase. This means that with $\Phi = \Phi_{\rm J}$ the atmosphere enters the rapid escape regime between 0.2 and 0.3 AU, i.e. slightly inwards from the corresponding transition for a planet with $\Phi = 0.5$ $\Phi_{\rm J}$. We note that the previous calculations of Koskinen *et al.* [23], who also used $\Phi = \Phi_{\rm J}$, placed this transition between 0.1 and 0.2 AU. The difference between the calculations here and the previous results could be due to circulation. With a slow rotation rate approaching tidal synchronization that was assumed by Koskinen *et al.* [23], the general circulation model at 0.2 AU develops strong day–night circulation at high altitudes that leads to upwelling in the dayside. This upwelling replenishes H_2 and helps to maintain the stability of the atmosphere. However, a faster rotation rate with a period of 24 h or less disturbs this type of circulation and leads to a transition to the rapid escape regime between 0.2 and 0.3 AU [42], in agreement with the one-dimensional globally averaged simulations presented here. It should be noted that, while close-in EGPs are assumed to be rotationally synchronized with their orbital periods [43], there is no reason to assume that this is the case further out between 0.2 and 0.3 AU.

With the surface potential increased to $\Phi = 3\Phi_{\rm J}$, the atmosphere at 0.2 AU does not undergo hydrodynamic escape. Instead, the exospheric temperature is only 2820 K with an exobase at 1.08 $R_{\rm p}$ and $X_\infty = 207$. At 0.1 AU, H_2 dissociates rapidly above the 1 μbar level, and the exospheric temperature increases to 12 400 K. However, even in this case, the exobase is at 1.5 $R_{\rm p}$ with $X_\infty = 33$ and the atmosphere does not escape hydrodynamically. At 0.05 AU, the exospheric temperature is 14 340 K and $X_\infty = 25$. These results confirm the finding of Koskinen *et al.* [34] that heavy planets such as HD17156b do not undergo rapid escape even at close-in orbits, despite the fact that H_2 is dissociated in their upper atmospheres.

Escape is less effective on heavier planets partly because radiative cooling offsets the stellar EUV heating near the heating peak. In our new calculations, we include cooling owing to recombination, but H Lyman α cooling can also contribute [44], keeping the temperature in the thermosphere close to 10 000 K. These cooling effects play a more significant role in the energy balance on planets with higher gravity, because the temperature in the thermosphere on such planets is not high enough for adiabatic cooling to become important. Further research is required to study the role of these cooling mechanisms in detail though as they are rarely included in models of giant planet atmospheres. In any case, our results show that a high-speed wind containing potassium atoms from the exosphere of another similar planet HD80606b, as proposed by Colón *et al*. [45], is unlikely to be realistic. The same considerations do not apply to planets such as GJ3470b with $\Phi = 0.1\ \Phi_{\rm J}$. We found that such planets undergo a transition to rapid escape much further out, and the exobase extends to very high altitude even at 1 AU.

Naturally, surface gravity also affects $\dot{M}_{\rm lim}$, which is directly proportional to the mass of the planet. Thus, the mass loss rate required to mix, say, C into the thermosphere of HD189733b is 1.7 times higher than on HD209458b. On HD17156b, the corresponding rate is 4.6 times higher than on HD209458b, and on GJ3470 it is 16 times lower than on HD209458b. Thus, the collisional mixing of heavy species is much more likely on planets with a low surface gravity than on heavy planets such as HD17156b. Given that the escape rates on HD17156b or HD80606b are likely to be comparable to the Jeans escape rate even at the periastron near 0.05 AU, we do not expect that substantial abundances of heavy elements escape from their atmospheres. Instead, heavy species on these planets are likely to be diffusively separated below the exobase.

4. Discussion and conclusion

The study of extrasolar planet atmospheres is still an emerging field. This means that there are many uncertainties in both the models and even the interpretation of the observations. For instance, we used T–P profiles in the lower atmosphere that are based on models that make many simplifying assumptions about the composition and radiative transfer [29,30]. Although these models account for condensation, cloud formation and the scattering of radiation, they ignore the effects of photochemistry and non-local thermodynamic equilibrium radiative transfer that can, for instance, produce strong emission features on close-in planets [46,47]. The temperature profile in the thermosphere, on the other hand, depends on the photoelectron heating efficiencies and the H_3^+ infrared cooling rates. Fully self-consistent calculations of the heating efficiency do not yet exist, and H_3^+ emissions have not been detected on EGPs. In fact, our estimates indicate that these emissions are undetectable with current instruments despite the fact that they can play a substantial role in the energy balance of EGPs.

The composition and T–P profiles are also affected by dynamics and turbulent mixing. There are no observational constraints on the impact of dynamics on the composition, and only a few constraints on circulation in general. Yet, dynamics can play a large role in the atmosphere, controlling processes such as cloud formation and the mixing ratios of heavy elements in the upper atmosphere. Photochemistry, dynamics and thermal structure are all driven by the stellar flux. It is surprising how little is known about the properties of the host stars and the details of their spectra. The activity cycle of even other Sun-like stars is not well understood although it is likely to affect both the atmospheres and the interpretation of transit observations. Even less is known about stars of other spectral type. For instance, M stars exhibit a range of activity levels, in general, and can be highly variable even on short time scales [48].

Despite the uncertainties, we are able to identify some robust qualitative results. First, there are two distinct regimes of atmospheric escape that are separated by a relatively sharp transition controlled by the stellar flux. In the 'stable' regime, stellar heating is balanced by downwards conduction and/or radiative cooling. In this case, the mass loss rate is typically many orders of magnitude smaller than the energy-limited escape rate that is based on the thermospheric heating efficiency. In the 'unstable' regime, stellar heating is efficient enough to cause a significant expansion of the atmosphere. As a result, stellar heating is balanced by adiabatic cooling, and the

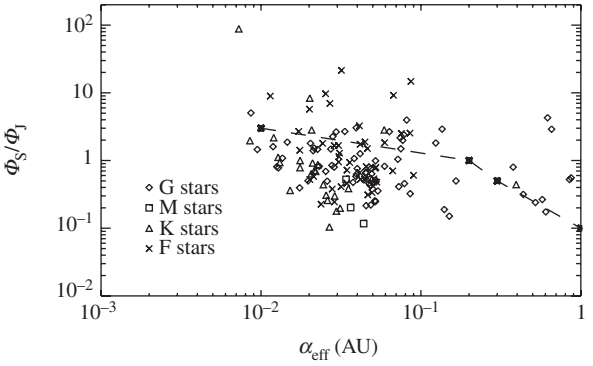

Figure 2. Surface potential of EGPs with known radius, mass and the spectral type of the host star as a function of effective orbital distance (see text). The dashed line shows the transition between unstable escape-dominated (to the left) and stable (to the right) regimes as defined in the text. The multiplication symbols show the values of Φ for which simulations were performed.

temperature decreases with altitude above the EUV heating peak. In this regime, the mass loss rate is comparable to the energy-limited mass loss rate that is based on the thermospheric heating efficiency. The transition between these two regimes on close-in EGPs is sharp, because it is, in many cases, driven by the dissociation of H_2. The H_2/H dissociation front is sharp both as a function of altitude in the atmospheric models and in terms of orbital distance.

In addition to stellar flux and composition, the escape mechanism depends on the surface gravitational potential. We find that planets such as HD209458b with $\Phi = 0.5\ \Phi_J$ are stable at orbital distances greater than about 0.3 AU. In our calculations, this corresponds to an integrated EUV flux of $F_{lim} = 44\,mW\,m^{-2}$ at wavelengths shorter than 912 Å. For planets such as Jupiter, this limit is closer at 0.2 AU ($F_{lim} = 0.1\,W\,m^{-2}$). The atmospheres of heavier planets such as HD17156b are stable even at 0.05 AU ($F_{lim} = 1.6\,W\,m^{-2}$), and unstable only near 0.01 AU. The atmospheres of planets such as GJ3470b are much more likely to escape hydrodynamically, even near 1 AU. The escape of heavy species is controlled by the escape rate of hydrogen. For a planet such as HD209458b, the energy-limited escape rate is high enough to cause species more massive than C to escape within 0.1 AU. The escape of heavy species from planets such as HD17156b is unlikely, whereas planets such as GJ3470b can start losing heavy species within 1 AU. We note here that we did not calculate photochemistry in the lower atmosphere for planets with different Φ, assuming that the changes in the mass and radius of the planet do not affect the H_2/H transition significantly.

To illustrate the results, figure 2 shows the gravitational potential $\Phi = GM_p/R_p$ of currently known transiting EGPs (planets with a mass higher than 10 M_E) as a function of effective orbital distance. This is the orbital distance in the Solar System where the planets would receive the same EUV flux as they do currently, given an estimate of the EUV flux of their host stars. For G stars, we used the solar flux ($4\,mW\,m^{-2}$ at 1 AU). When an estimate of the stellar age exists, we scaled the flux according to equation (1) of Ribas *et al*. [49]. For M, K and F stars, we used the simple scaling proposed by Lecavelier des Etangs [24] without accounting for a possible age dependence. We excluded planets for which the spectral type of the host star is not listed at www.exoplanet.eu. The names of the planets in figure 2 can be made available on request.

Our results indicate that most of the transiting EGPs have rapidly escaping atmospheres, and heavy species are expected to escape with H on many of the currently known planets. However, this is not true of the heavier planets such as HD17156b or HD80606b, even if they come close to the host star. There is also an intermediate region in figure 2 where hydrogen is escaping rapidly, but heavier species are still likely to be diffusively separated and not escape the atmosphere with large abundances. It is interesting that there are no planets within 0.01–0.03 AU. Garcia Munoz [33] pointed out that the mass loss rate increases very steeply with decreasing orbital

distance within 0.015 AU owing to stellar gravity. At such orbital distance, the interaction of the planet with the stellar wind is also expected to be more violent. In this context, it is important to note that our work does not include stellar gravity or any additional escape mechanisms such as erosion by the stellar wind. Our results are intended to provide constraints on the thermal escape rate and mechanism that can be used as a base of more complex models in the future when more detailed observations are available to characterize the complex physics of atmospheric escape.

Based on estimates of the stellar flux and Φ, the limits given in figure 2 can be used to determine the thermal escape mechanism for different EGPs. We note, however, that the limits for the different escape regimes here are based on models with a relatively few values of $a_{\rm eff}$ and Φ, and we recommend that interested readers contact the authors for separate models of specific targets if more accurate results are required. We also stress that only a detailed comparison of the simulations with actual observations can validate the models, and future efforts in characterizing the upper atmospheres of EGPs should concentrate on obtaining multiple observations of both the host stars and the planets in different systems, and designing new techniques and instruments to make these observations possible.

Acknowledgements. The calculations in this paper relied on the high performance astrophysics simulator (HiPAS) at the University of Arizona, and the University College London Legion High Performance Computing Facility, which is part of the DiRAC Facility jointly supported by STFC and the Large Facilities Capital Fund of BIS. SOLAR2000 Professional Grade V2.28 irradiances were provided by Space Environment Technologies.
Funding statement. This research was supported by the National Science Foundation grant no. AST1211514.

References

1. Vidal-Madjar A, Lecavelier des Etangs A, Désert J-M, Ballester GE, Ferlet R, Hébrard G, Mayor M. 2003 An extended upper atmosphere around the extrasolar giant planet HD209458b. *Nature* **422**, 143–146. (doi:10.1038/nature01448)
2. Vidal-Madjar A *et al*. 2004 Detection of oxygen and carbon in the hydrodynamically escaping atmosphere of the extrasolar planet HD209458b. *Astrophys. J. Lett.* **604**, L69–L72. (doi:10.1086/383347)
3. Linsky JL, Yang H, France K, Froning CS, Green JC, Stocke JT, Osterman SN. 2010 Observations of mass loss from the transiting exoplanet HD209458b. *Astrophys. J.* **717**, 1291–1299. (doi:10.1088/0004-637X/717/2/1291)
4. Fossati L *et al*. 2010 Metals in the exosphere of the highly irradiated planet WASP-12b. *Astrophys. J. Lett.* **714**, L222–L227. (doi:10.1088/2041-8205/714/2/L222)
5. Lecavelier des Etangs A *et al*. 2010 Evaporation of the planet HD189733b observed in H I Lyman α. *Astron. Astrophys.* **514**, A72. (doi:10.1051/0004-6361/200913347)
6. Lecavelier des Etangs A *et al*. 2012 Temporal variations in the evaporating atmosphere of the exoplanet HD189733b. *Astron. Astrophys. Lett.* **543**, L4. (doi:10.1051/0004-6361/201219363)
7. Koskinen TT, Yelle RV, Lavvas P, Lewis N. 2010 Characterizing the thermosphere of HD209458b with UV transit observations. *Astrophys. J.* **723**, 116–128. (doi:10.1088/0004-637X/723/1/116)
8. Koskinen TT, Harris MJ, Yelle RV, Lavvas P. 2013 The escape of heavy atoms from the ionosphere of HD209458b. I. A photochemical–dynamical model of the thermosphere. *Icarus* **226**, 1678–1694. (doi:10.1016/j.icarus.2012.09.027)
9. Koskinen TT, Yelle RV, Harris MJ, Lavvas P. 2013 The escape of heavy atoms from the ionosphere of HD209458b. II. Interpretation of the observations. *Icarus* **226**, 1695–1708. (doi:10.1016/j.icarus.2012.09.026)
10. Lammer H, Selsis F, Ribas I, Guinan EF, Bauer SJ, Weiss WW. 2003 Atmospheric loss of exoplanets resulting from stellar X-ray and extreme-ultraviolet heating. *Astrophys. J. Lett.* **598**, L121–L124. (doi:10.1086/380815)
11. Yelle RV. 2004 Aeronomy of extra-solar giant planets at small orbital distances. *Icarus* **170**, 167–179. (doi:10.1016/j.icarus.2004.02.008)
12. Parker EN. 1958 Dynamics of the interplanetary gas and magnetic fields. *Astrophys. J.* **128**, 664–676. (doi:10.1086/146579)

13. Erkaev NV, Lammer H, Kulikov YuN, Langmayr D, Selsis F, Jaritz GF, Biernat HK. 2007 Roche lobe effects on the atmospheric loss from 'hot Jupiters'. *Astron. Astrophys.* **472**, 329–334. (doi:10.1051/0004-6361:20066929)
14. Stone JM, Proga D. 2009 Anisotropic winds from close-in extrasolar planets. *Astrophys. J.* **694**, 205–213. (doi:10.1088/0004-637X/694/1/205)
15. Trammell GB, Arras P, Li Z-Y. 2011 Hot Jupiter magnetospheres. *Astrophys. J.* **728**, 152. (doi:10.1088/0004-637X/728/2/152)
16. Tian F, Kasting JF, Liu H-L, Roble RG. 2008 Hydrodynamic planetary thermosphere model: 1. Response of the Earth's thermosphere to extreme solar EUV conditions and the significance of adiabatic cooling. *J. Geophys. Res.* **113**, E05008. (doi:10.1029/2007JE002946)
17. Tian F, Solomon SC, Qian L, Lei J, Roble RG. 2008 Hydrodynamic planetary thermosphere model: 2. Coupling of an electron transport/energy deposition model. *J. Geophys. Res.* **113**, E07005. (doi:10.1029/2007JE003043)
18. Strobel DF. 2002 Aeronomic systems on planets, moons, and comets. In *Atmospheres in the solar system: comparative aeronomy* (eds M Mendillo, A Nagy, H Waite). Geophys. Monogr. Ser. no. 130, pp. 7–22. Washington, DC: AGU.
19. Koskinen TT, Sandel BR, Yelle RV, Capalbo FJ, Holsclaw GM. 2013 The density and temperature structure near the exobase of Saturn from Cassini UVIS solar occultations. *Icarus* **226**, 1318–1330. (doi:10.1016/j.icarus.2013.07.037)
20. Volkov AN, Johnson RE, Tucker OJ, Erwin JT. 2011 Thermally driven atmospheric escape: transition from hydrodynamic escape to Jeans escape. *Astrophys. J. Lett.* **729**, L24. (doi:10.1088/2041-8205/729/2/L24)
21. Volkov AN, Tucker OJ, Erwin JT, Johnson RE. 2011 Kinetic simulations of thermal escape from a single component atmosphere. *Phys. Fluids* **23**, 066601. (doi:10.1063/1.3592253)
22. Koskinen TT, Aylward AD, Miller S, Smith CGA. 2007 A thermospheric circulation model for extrasolar giant planets. *Astrophys. J.* **661**, 515–526. (doi:10.1086/513594)
23. Koskinen TT, Aylward AD, Miller S. 2007 A stability limit for the atmospheres of giant extrasolar planets. *Nature* **450**, 845–848. (doi:10.1038/nature06378)
24. Lecavelier des Etangs A. 2007 A diagram to determine the evaporation status of extrasolar planets. *Astron. Astrophys.* **461**, 1185–1193. (doi:10.1051/0004-6361:20065014)
25. Lammer H *et al*. 2009 Determining the mass loss limit for close-in exoplanets: what can we learn from transit observations? *Astron. Astrophys.* **506**, 399–410. (doi:10.1051/0004-6361/200911922)
26. Moses JI *et al*. 2011 Disequilibrium carbon, oxygen, and nitrogen chemistry in the atmospheres of HD189733b and HD209458b. *Astrophys. J.* **737**, 15. (doi:10.1088/0004-637X/737/1/15)
27. Lavvas P, Coustenis A, Vardavas IM. 2008 Coupling photochemistry with haze formation in Titan's atmosphere, part I: model description. *Planet. Space Sci.* **56**, 27–66. (doi:10.1016/j.pss.2007.05.026)
28. Lavvas P, Coustenis A, Vardavas IM. 2008 Coupling photochemistry with haze formation in Titan's atmosphere, part II: results and validation with Cassini/Huygens data. *Planet. Space Sci.* **56**, 67–99. (doi:10.1016/j.pss.2007.05.027)
29. Sudarsky D, Burrows A, Hubeny I. 2003 Theoretical spectra and atmospheres of extrasolar giant planets. *Astrophys. J.* **588**, 1121–1148. (doi:10.1086/374331)
30. Burrows A, Sudarsky D, Hubeny I. 2004 Spectra and diagnostics for the direct detection of wide-separation extrasolar giant planets. *Astrophys. J.* **609**, 407–416. (doi:10.1086/420974)
31. Showman AP, Fortney JJ, Lian Y, Marley MS, Freedman RS, Knutson HA, Charbonneau D. 2009 Atmospheric circulation of hot Jupiters: coupled radiative-dynamical general circulation model simulations of HD189733b and HD209458b. *Astrophys. J.* **699**, 564–584. (doi:10.1088/0004-637X/699/1/564)
32. Koskinen TT, Cho JY-K, Achilleos N, Aylward AD. 2010 Ionization of extrasolar giant planet atmospheres. *Astrophys. J.* **722**, 178–187. (doi:10.1088/0004-637X/722/1/178)
33. Garcia Munoz A. 2007 Physical and chemical aeronomy of HD209458b. *Planet. Space Sci.* **55**, 1426–1455. (doi:10.1016/j.pss.2007.03.007)
34. Koskinen TT, Aylward AD, Miller S. 2009 The upper atmosphere of HD17156b. *Astrophys. J.* **693**, 868–885. (doi:10.1088/0004-637X/693/1/868)
35. Seiff A *et al*. 1998 Thermal structure of Jupiter's atmosphere near the edge of a 5 μm hot spot in the north equatorial belt. *J. Geophys. Res.* **103**, 22 857–22 889. (doi:10.1029/98JE01766)

36. Miller S, Aylward AD, Millward G. 2005 Giant planet ionospheres and thermospheres: the importance of ion-neutral coupling. *Space Sci. Rev.* **116**, 319–343. (doi:10.1007/s11214-005-1960-4)
37. Müller-Wodarg ICF, Mendillo M, Yelle RV, Aylward AD. 2006 A global circulation model of Saturn's thermosphere. *Icarus* **180**, 147–160. (doi:10.1016/j.icarus.2005.09.002)
38. Smith CGA, Aylward AD, Millward GH, Miller S, Moore LE. 2007 An unexpected cooling effect in Saturn's upper atmosphere. *Nature* **445**, 399–401. (doi:10.1038/nature05518)
39. Torr MR, Richards PG, Torr DG. 1981 Solar EUV energy budget of the thermosphere. *Adv. Space Res.* **1**, 53–61. (doi:10.1016/0273-1177(81)90417-8)
40. Gross SH. 1972 On the exospheric temperature of hydrogen-dominated planetary atmospheres. *J. Atmos. Phys.* **29**, 214–218. (doi:10.1175/1520-0469(1972)029<0214:OTETOH>2.0.CO;2)
41. Hunten DM, Pepin RO, Walker JCG. 1987 Mass fractionation in hydrodynamic escape. *Icarus* **69**, 532–549. (doi:10.1016/0019-1035(87)90022-4)
42. Koskinen TT. 2008 Stability of short period exoplanets. PhD thesis, University College London, London, UK.
43. Guillot T, Burrows A, Hubbard WB, Lunine JI, Saumon D. 1996 Giant planets at small orbital distances. *Astrophys. J. Lett.* **459**, L35–L38. (doi:10.1086/309935)
44. Murray-Clay RA, Chiang EI, Murray N. 2009 Atmospheric escape from hot Jupiters. *Astrophys. J.* **693**, 23–42. (doi:10.1088/0004-637X/693/1/23)
45. Colón KD, Ford EB, Redfield S, Fortney JJ, Shabram M, Deeg HJ, Mahadevan S. 2012 Probing potassium in the atmosphere of HD80606b with tunable filter transit spectrophotometry from the Gran Telescopio Canarias. *Mon. Not. R. Astron. Soc.* **419**, 2233–2250. (doi:10.1111/j.1365-2966.2011.19878.x)
46. Swain MR *et al*. 2010 A ground-based near-infrared emission spectrum of the exoplanet HD189733b. *Nature* **463**, 637–639. (doi:10.1038/nature08775)
47. Waldmann IP, Tinetti G, Drossart P, Swain MR, Deroo P, Griffith CA. 2012 Ground-based near-infrared emission spectroscopy of HD189733b. *Astrophys. J.* **744**, 35. (doi:10.1088/0004-637X/744/1/35)
48. France K *et al*. 2013 The ultraviolet radiation environment around M dwarf exoplanet host stars. *Astrophys. J.* **763**, 149. (doi:10.1088/0004-637X/763/2/149)
49. Ribas I, Guinan EF, Güdel M, Audard M. 2005 Evolution of the solar activity over time and effects on planetary atmospheres. I. High-energy irradiances (1–1700 Å). *Astrophys. J.* **622**, 680–694. (doi:10.1086/427977)